JMEPEG (2009) 18:1046–1051
DOI: 10.1007/s11665-008-9350-1

1059-9495/$19.00

Growth of AlN Films and Its Process Development for the Fabrication of Acoustic Devices and Micromachined Structures

J.P. Kar, G. Bose, S. Tuli, A. Dangwal, and S. Mukherjee

(Submitted December 13, 2007; in revised form November 4, 2008)

AlN films were grown on silicon substrates by RF reactive magnetron sputtering. At high sputtering powers, (002) preferred orientation as well as Al-N absorption band becomes prominent. The surface roughness and grain size of sputtered films were found to increase with RF power. Surface acoustic wave (SAW) device has been made on the grown (002) oriented piezoelectric AlN film with interdigital transducer (IDT) electrodes spacing corresponding to a wavelength of 60 µm. The centre frequency of the SAW filter was found to be 84.304 MHz, which gives a phase velocity of 5058 m/s with an electromechanical coupling coefficient (K^2) of 0.34%. Low etch rate of AlN films were observed in doped TMAH solution. Three-dimensional suspended Cr/AlN/Cr/SiO_2 microstructures were also fabricated by wet chemical etching.

Keywords AlN, etching, SAW, sputtering

1. Introduction

Surface acoustic wave (SAW) and bulk acoustic wave (BAW) devices are widely used in wireless communication industry (Ref 1, 2). These devices can be realized either on a solid substrate/film or through micromachined suspended structures. In SAW devices, an elastic wave travels on the surface of a piezoelectric material. Elastic waves in a solid are produced through Interdigital Transducer (IDT) placed on the piezoelectric material. These devices are typically made on single crystal piezoelectric substrates, such as quartz, lithium niobate, and lithium tantalate (Ref 3). Unfortunately, these piezoelectric substrates-based devices have a variety of limitations for high frequency device fabrication: in particular, low acoustic wave velocity and lithography constraint. In addition, as these electroacoustic devices are made on single crystal piezoelectric substrates, they cannot be monolithically integrated with semiconductor substrates used in IC technology. On the other hand, thin film bulk acoustic resonators (TFBARs), with a piezoelectric material sandwiched between two electrodes, have gained attention for high frequency applications. Hence, thin film electronic materials are actively under consideration to meet these issues (Ref 4). In general, piezoelectric thin films such as aluminum nitride (AlN), zinc oxide (ZnO), and lead zirconium titanate (PZT), which are polycrystalline in nature, are used for high frequency SAW devices and TFBARs (Ref 5-8). AlN has higher SAW velocity, lower propagation loss, and higher thermal stability, which can be grown on various substrates (Ref 9, 10). Furthermore, it is essential that the growth and the processing of these films are compatible to the complementary metal oxide semiconductor (CMOS) process and can be used as an integral part of the IC chip. Among various deposition techniques, sputtering has many advantages for thin film growth because of its simplicity, low thermal budget and ability to obtain good quality films with desired properties.

To realize BAW resonators, especially those using suspended microstructures, silicon micromachining is often required (Ref 11, 12). The etchants, commonly used for silicon micromachining such as potassium hydroxide (KOH) or ethylenediamine pyrochatechol (EDP), are not suitable to realize AlN-based microstructures, because these chemicals readily attack Al and AlN films (Ref 13). For AlN film-based MEMS devices people are generally using a specially designed mask for both Al and AlN layers or KOH etching before AlN film deposition and then for the rest of the silicon etching by inductively coupled plasma (ICP) technique after deposition and patterning of all constituent films (Ref 11, 14). These techniques are not well suited for IC processing. A technique, which is more versatile, CMOS process-compatible, nontoxic and also able to provide better selective etching with doped tetramethylammonium hydroxide (TMAH) etchant, is reportedly in the development stage (Ref 15). Herein, we investigated the growth of *c*-axis-oriented AlN film, fabrication, and characterization of SAW device and selective silicon etching by doped TMAH to realize AlN-based microstructures.

2. Experimental

Aluminum nitride films were synthesized by RF reactive magnetron sputtering (Alcatel SCM 450) from a pure aluminum target (6-in. diameter) in a high purity argon and nitrogen

J.P. Kar, G. Bose, and **S. Tuli**, Centre for Applied Research in Electronics, I. I. T. Delhi, New Delhi 110 016, India; **A. Dangwal**, Department of Physics, I. I. T. Delhi, New Delhi 110 016, India; and **S. Mukherjee**, School of Electrical and Computer Engineering, University of Oklahoma, Norman 73019. Contact e-mail: karjp@rediffmail.com.

gas mixture. P-type (100)-Si wafers of resistivity 8-12 ohm cm, was used as substrates. Prior to loading silicon substrates into the sputter chamber, the Si substrates were cleaned in isopropyl alcohol (IPA). Thereafter, the wafers were kept in a solution of H_2SO_4:H_2O_2 (1:1) for 10 min and then dipped into a dilute solution of 5% HF to remove the surface oxide. After such cleaning, the substrates were rinsed in deionized water and blow-dried in N_2. Bruker (D-8) X-ray diffractometer (XRD) was used to characterize the crystallinity of AlN films. FTIR spectra were obtained with Nicolet Spectrometer (Impact 410). Surface morphology of the grown films was studied by scanning electron microscope (Cambridge instruments, Stereoscan 360) and atomic force microscope (Thermomicroscope, CP research system) in contact mode (2×2 μm^2). Due to the low etching selectivity between Al and AlN, gold/chrome contacts were deposited for realization of IDTs. Au/Cr films were deposited on the AlN/Si film and the IDTs were realized after standard lithography and etching processes. SAW devices were fabricated with normal finger IDTs, each with 25 finger pairs of 60 μm wavelength, aperture of 5 mm, and inter IDT spacing of 7 mm. The SAW frequency response of the Au-Cr(IDT)/AlN/Si structures was measured by a Rohde & Schwarz ZVK network analyzer.

In separate experiments, windows were opened in AlN film by photolithography and etching processes used in silicon micromachining. Commercially available TMAH (25 wt.% water solution, Qualigens) was diluted to reduce its concentration (TMAH, 5 wt.%). This solution was then doped with silicic acid (30.5 g/L) and ammonium persulphate (5.5 g/L). To protect Al and AlN, silicic acid has been chosen instead of pure silicon powder, because silicic acid tends to dissolve quickly in TMAH solution. Thereafter, ammonium persulphate (AP) was added to the abovementioned solution to reduce the surface roughness of etched silicon. All experiments were carried out in a glass container equipped with water-cooled condenser at 85 °C in a constant temperature oil bath. Diluted HF cannot be used to remove native oxides from the surface of the wafer as it readily attacks aluminum (Al) layer. Therefore, native oxide was removed using a special native oxide etchant (ammonium fluoride, acetic acid, ethylene glycol, and DI water solution). Etch rates of AlN film and silicon were measured by Filmemetrics (F 20) and α-step (100), respectively.

3. Results and Discussion

3.1 AlN Growth and Characterization

The properties AlN films depend on the kinetics of the sputtered species, which can be altered by varying the growth parameters. In this study, investigations have been made to get a better quality AlN film for acoustic devices. Structural properties of AlN films deposited on silicon were studied with varying RF sputtering power from 100 to 400 W. In all the cases, film thickness was kept around 300 nm. At 100 W, the films were amorphous. When sputtering power was increased to a range of 200-300 W, films with (002) orientation were observed. On increasing the power further to 400 W, a significant orientation has taken place. This may be due to the increase in adatom energy with RF power, which favors formation of well-oriented (002) Al-N films (Ref 16, 17). The transmission spectra, recorded by a Fourier Transform Infrared (FTIR) spectrophotometer at normal incidence, was in the range from 400 to 3000 cm^{-1}. Figure 1 shows the characteristic absorption band of Al-N at 682 cm^{-1}. As the sputtering power is increased, the peak corresponding to the Al-N stretching mode becomes prominent and narrows down substantially. Narrowing of a vibrational band generally indicates better crystallinity with the decrease in short-range order (Ref 18). Effect of sputtering power on the surface roughness and grain size has been studied by AFM and SEM, respectively. Since no crystallinity was observed for 100 W, its morphological properties were not investigated. Figure 2 plots the 2-D AFM images measured by AFM (contact mode) on 2×2 μm^2, area with the increase in sputtering power from 200 to 400 W. The roughness of the films increases from 1.62 to 3.04 nm with RF power, which confirms better surface mobility of the adatoms at high RF power, resulting in growth of grain size (Ref 16, 19). This is also evident from the scanning electron micrographs as shown in Fig. 3. Similarly, other sputtering parameters were optimized in different set of experiments. Relatively highly *c*-axis (002)-oriented films were found in between 200 and 300 °C (Ref 20). It was found that the crystallinity of (002) orientation of the AlN film gradually increased till 6×10^{-3} mbar, but changed to the (100) crystal orientation at 8×10^{-3} mbar (Ref 21). It was revealed that both (002) crystallographic orientation and the FTIR absorption peak became prominent with increase in nitrogen concentration (Ref 22). Crystallinity enhanced significantly for the films grown at a lower target to substrate distance (5 cm). The optimized growth parameters of AlN films are listed in Table 1. Well-oriented polycrystalline AlN films (0.92 μm) were deposited by reactive RF magnetron sputtering technique on Si (100) substrate. *c*-Axis (002)-oriented peak is recorded at 2θ value of 36.1° (Fig. 4), which reflects the piezoelectric nature of the AlN film. The inset of the figure shows the columnar growth of AlN films and this result supports the XRD observations.

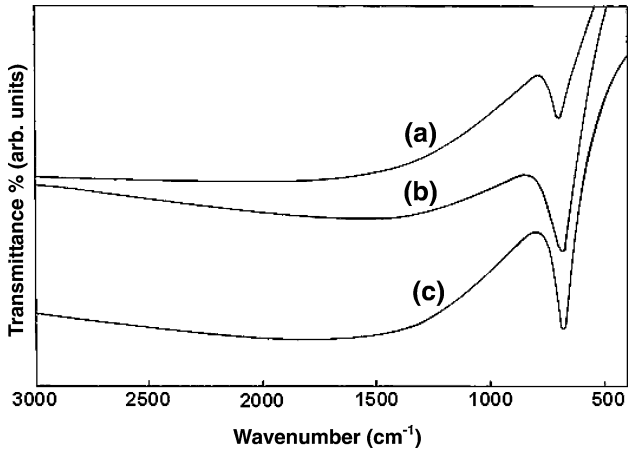

Fig. 1 FTIR transmission spectra of AlN films deposited at (a) 200 W, (b) 300 W, (c) 400 W

3.2 SAW Processing and Characterization

The SAW device response is shown in Fig. 5. The thickness of the AlN film used for the fabrication of SAW device was 0.92 μm. The start and stop frequencies in the network analyzer measurement are 60 MHz and 109 MHz, respectively. The SAW device parameters are centre frequency (84.304 MHz), SAW velocity (5058 m/s), and electromechanical coupling coefficient (K^2 = 0.34%), taking into account the wavelength of

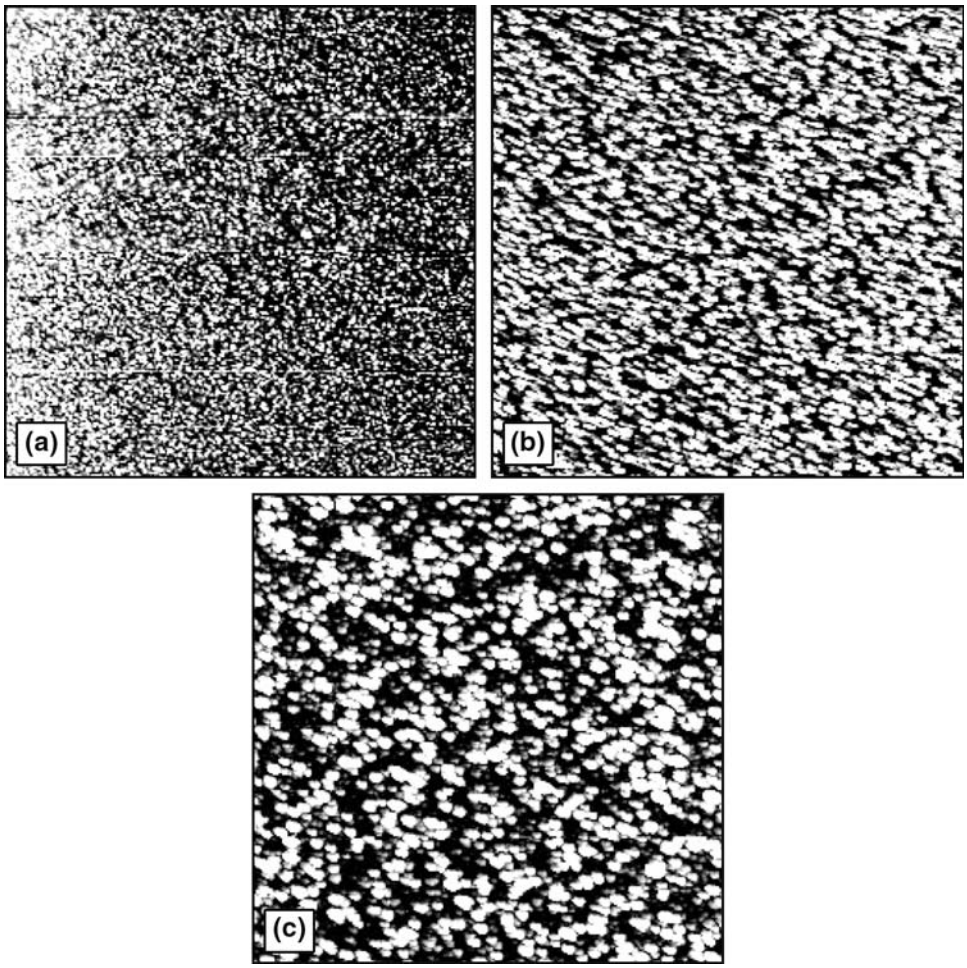

Fig. 2 AFM image of sputter-deposited AlN films deposited at (a) 200 W, (b) 300 W, (c) 400 W

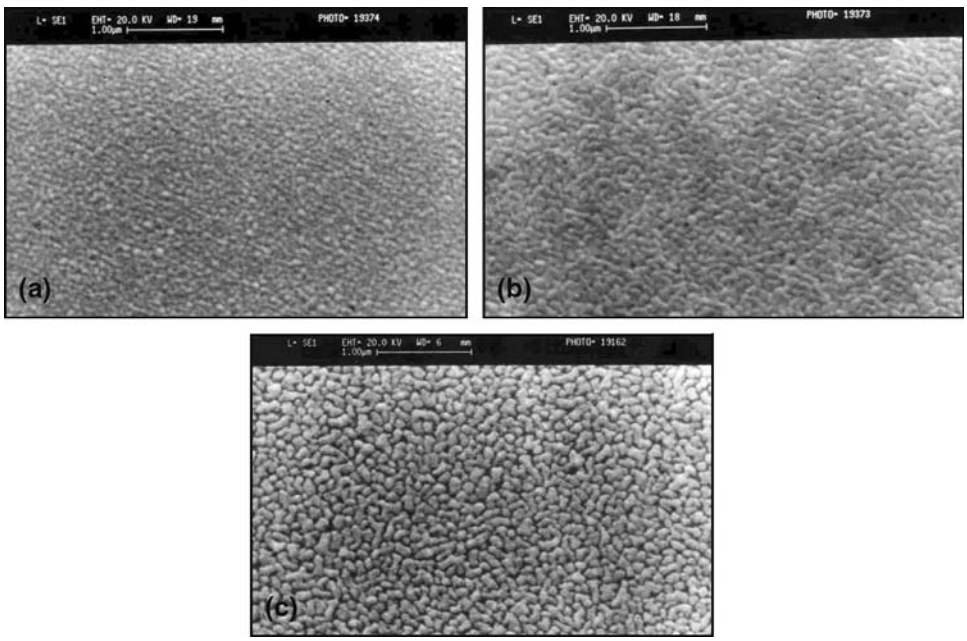

Fig. 3 SEM micrographs of AlN films deposited at (a) 200 W, (b) 300 W, (c) 400 W

Table 1 Optimal deposition parameters of AlN films

Base vacuum	3×10^{-6} mbar
Target	Al (99.99%)
Sputtering gas	Ar (99.999%)
Reactive gas	N_2 (99.999%)
Gas flow ratio	Ar:N_2 = 1:4
Sputtering pressure	6×10^{-3} mbar
Substrate temperature	200 °C
RF power	400 W

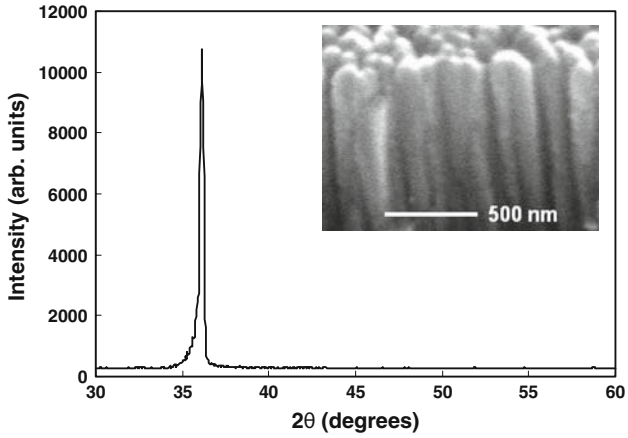

Fig. 4 X-ray diffraction diagram of an AlN-deposited in the optimal deposition conditions. Inset: SEM picture in cross section that shows the columnar structure of the *c*-axis oriented AlN films

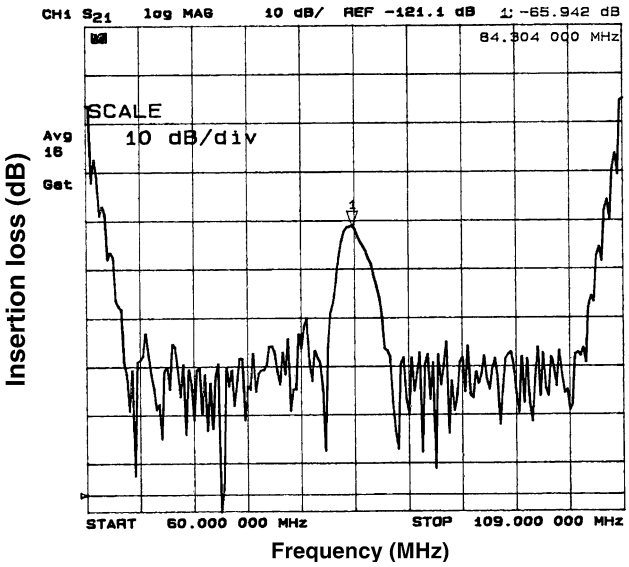

Fig. 5 Frequency response of AlN-based SAW device

60 μm. While the first one is directly measured, the latter two (velocity and electromechanical coupling coefficient) are estimated from the measured frequency response (Ref 23, 24).

3.3 Micromachining

After photolithography, windows were opened by etching SiO_2, Al, and AlN layers, where SiO_2, AlN, and Al films were etched by BHF, 0.6% TMAH, and a mixture of chemicals

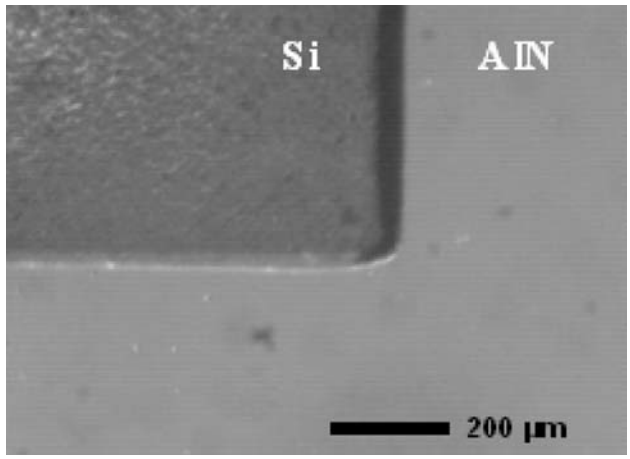

Fig. 6 Micrographs of etched silicon with AlN film as masking layer

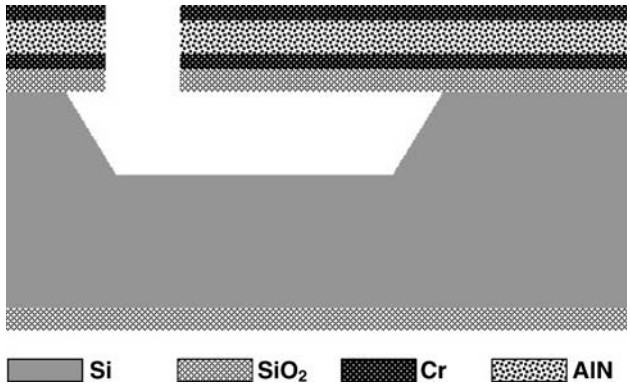

Fig. 7 Layout of Cr/AlN/Cr/SiO_2 microstructures

(H_3PO_4, HNO_3, CH_3COOH, H_2O), respectively. Silicon was etched through the windows using doped TMAH solution. Herein, SiO_2, Al, and AlN films were used as mask layers. Figure 6 shows the micrographs of the cavity in silicon after silicon micromachining. The etch rate of silicon in doped TMAH is 50 μm/h. Low etch rates of AlN (18-30 nm/h) was found to be encouraging for MEMS applications. It is interesting to note that dilute TMAH is a well-known etchant for AlN film and Al as well (Ref 25). But doped TMAH shows significantly lower etch rates for AlN, which can be exploited for three-dimensional microstructures fabrication. Probable reason for low etch rate of AlN is the formation of a passivating layer during TMAH etching (Ref 26, 27). Doped TMAH solution has the decreased pH value and, therefore, reduces the number of free hydroxyl ions and the etch rate of silicon oxides. On the other hand, Al films (handled at air) are covered by a thin aluminum oxide film. Schnakenberg et al. reported that the silicates in the solution react with $Al(OH)_3$ to form sparingly soluble pyrophyllite-type silicates which passivate the aluminum oxide surface (Ref 28). However, for the AlN layer, the mechanism is still unclear and requires further research. This technique can be used to remove the silicon under the silicon dioxide film to realize Cr/AlN/Cr/SiO_2 beam, where silicon dioxide films were thermally grown on silicon substrate (Fig. 7). In addition, the AlN and Cr films were grown by RF sputtering. Micropatterns of stack layers on the front side of

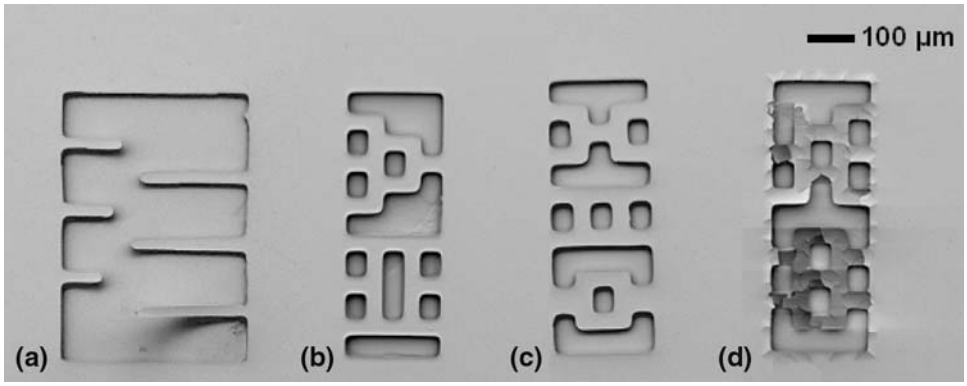

Fig. 8 Micrographs of Cr/AlN/Cr/SiO_2/Si cantilevers and microstructures

the wafer were made by standard IC photolithography and etching process. Herein, two-step etching was carried out by the combination of both isotropic and anisotropic etching in order to realize suspended microstructures and to reduce hillocks. Before insertion of the samples in doped TMAH solution, native oxide was removed by 5% HF dip. Thereafter, etching was carried out in doped TMAH at 85 °C in a reflux container. After anisotropic silicon etching by doped TMAH solution, the wafers were placed for isotropic etching of silicon in a mixture of ammonium fluoride (5 parts), nitric acid (120 parts), and DI water (60 parts) at room temperature to reduce hillocks. The portion under the Cr/AlN/Cr/SiO_2 goes away with increasing etching duration leaving behind the suspended Cr/AlN/Cr/SiO_2 structures. Cavity depth was maintained at about 20 μm in order to avoid any kind of stiction after the release of microstructures. Undercutting of silicon at the boundary of the cavity is also observed. One has to take this into account during device design. Figure 8 shows different types of microstructures obtained by both types of etching. Figure 8(a) depicts suspended cantilevers fixed at one end, wherein one of the microstructures lifted up because of the stress. Various kinds of AlN-based microstructures with two ends fixed are shown in Fig. 8(b) and (c). Collapse of microstructures by electric charges confirms that the construction of these structures is fully suspended (Fig. 8d). The charge on the microstructures was generated by SEM electron beam, accelerated by a potential of 20 KV. However, further research is required for the precise control of undercutting as well as the reduction of hillocks during the use of TMAH.

4. Conclusion

AlN films were grown on silicon substrates by RF-reactive magnetron sputtering. At higher sputtering powers, (002)-preferred orientation as well as Al-N absorption band becomes prominent. The surface roughness and grain size of sputtered films were found to increase with RF power. The SAW device is demonstrated on the grown (002)-oriented AlN film. The centre frequency of the SAW filter was found to be 84.304 MHz, which gives a phase velocity of 5058 m/s with K^2 of 0.34%. Low etch rate of AlN films were observed in doped TMAH solution. Doped TMAH shows significantly lower etch rates for AlN and Al, which can be exploited for the fabrication of AlN-based micro-electro-mechanical systems (MEMS).

Acknowledgment

The authors are thankful to Prof. D. T. Shahani for the valuable discussions and support extended by him during the course of this research study.

References

1. K.M. Lakin, A Review of Thin-Film Resonator Technology, *IEEE Microw. Mag.*, December 2003, p 61–67
2. M.B. Assouar, O. Elmazria, M. El Hakiki, P. Alnot, and C. Tiusan, Low Temperature AlN Thin Films Growth for Layered Structure SAW and BAW Devices, *14th IEEE International Symposium on Applications of Ferroelectrics (ISAF-4)*, 23–27 August 2004, p 43–46
3. M.B. Assouar, M. El Hakiki, O. Elmazria, P. Alnot, and C. Tiusan, Synthesis and Microstructural Characterisation of Reactive RF Magnetron Sputtering AlN Films for Surface Acoustic Wave Filters, *Diamond Relat. Mater.*, 2004, **13**, p 1111–1115
4. S. Bender, F.L. Dickert, W. Mokwa, and P. Pachatz, Investigations on Temperature Controlled Monolithic Integrated Surface Acoustic Wave (SAW) Gas Sensors, *Sens. Actuators B*, 2003, **93**, p 164–168
5. H.P. Loebl, M. Klee, C. Metzmacher, W. Brand, R. Milsom, and P. Lok, Piezoelectric Thin AlN Films for Bulk Acoustic Wave (BAW) Resonators, *Mater. Chem. Phys.*, 2003, **79**, p 143–146
6. H. Yamada, Y. Ushimi, M. Takeuchi, Y. Yoshino, T. Makino, and S. Arai, Improvement of Crystallinity of ZnO Thin Film and Electrical Characteristics of Film Bulk Acoustic Wave Resonator by Using Pt Buffer Layer, *Vacuum*, 2004, **74**, p 689–692
7. M. Schreiter, R. Gabl, D. Pitzer, R. Primig, and W. Wersing, Electro-Acoustic Hysteresis Behaviour of PZT Thin Film Bulk Acoustic Resonators, *J. Eur. Ceram. Soc.*, 2004, **24**, p 1589–1592
8. Z. Li and W. Gao, ZnO Thin Films with DC and RF Reactive Sputtering, *Mater. Lett.*, 2004, **58**, p 1363–1370
9. B. Paci, A. Generosi, V.R. Albertini, M. Benetti, D. Cannatá, F.D. Pietrantonio, and E. Verona, A Study of Highly *c*-Axis Oriented AlN Films for Diamond-Based Surface Acoustic Wave Devices: Bulk Structure and Surface Morphology, *Sens. Actuators A*, 2007, **137**, p 279–286
10. I. Ingrosso, S. Petroni, D. Altamura, M. De Vittorio, C. Combi, and A. Passaseo, Fabrication of AlN/Si SAW Delay Lines with Very Low RF Signal Noise, *Microelectron. Eng.*, 2007, **84**, p 1320–1324
11. M. Benetti, D. Cannatà, F. Di Pietrantonio, V. Foglietti, and E. Verona, Microbalance Chemical Sensor Based on Thin-Film Bulk Acoustic Wave Resonators, *Appl. Phys. Lett.*, 2005, **87**, p. 173504
12. J. Olivares, E. Iborra, M. Clement, L. Vergara, J. Sangrador, and A. Sanz-Hervás, Piezoelectric Actuation of Microbridges Using AlN, *Sens. Actuators A*, 2005, **123–124**, p 590–595
13. P.J. French, Integration of Silicon MEMS Devices: Materials and Processing Considerations, *Smart Mater. Bull.*, January 2001, p 7–13
14. C.L. Huang, K.W. Tay, and L. Wu, Fabrication and Performance Analysis of Film Bulk Acoustic Wave Resonators, *Mater. Lett.*, 2005, **59**, p 1012–1016

15. R. Mukhiya, A. Bagolini, B. Margesin, M. Zen, and S. Kal, (100) Bar Corner Compensation for CMOS Compatible Anisotropic TMAH Etching, *J. Micromech. Microeng.*, 2006, **16**, p 2458–2462
16. H. Cheng and P. Hing, The Evolution of Preferred Orientation and Morphology of AlN Films Under Various RF Sputtering Powers, *Surf. Coat. Technol.*, 2003, **167**, p 297–301
17. C. Cheng, Y. Chen, H. Wang, and W. Chen, Low-Temperature Growth of Aluminum Nitride Thin Films on Silicon by Reactive Radio Frequency Magnetron Sputtering, *J. Vac. Sci. Technol. A*, 1996, **14**, p 2238–2242
18. C.L. Aardahl, J.W. Rogers Jr., H.K. Yun, Y. Ono, D.J. Tweet, and S.T. Hsu, Electrical Properties of AlN Thin Films Deposited at Low Temperature on Si(100), *Thin Solid Films*, 1999, **346**, p 174–180
19. K. Kusaka, D. Taniguchi, T. Hanabusa, and K. Tominaga, Effect of Input Power on Crystal Orientation and Residual Stress in AlN Film Deposited by dc Sputtering, *Vacuum*, 2000, **59**, p 806–813
20. J.P. Kar, G. Bose, and S. Tuli, Correlation of Electrical and Morphological Properties of Sputtered Aluminum Nitride Films with Deposition Temperature, *Curr. Appl. Phys.*, 2006, **6**, p 873–876
21. J.P. Kar, G. Bose, and S. Tuli, A Study on the Interface and Bulk Charge Density of AlN Films with Sputtering Pressure, *Vacuum*, 2006, **81**, p 494–498
22. J.P. Kar, G. Bose, and S. Tuli, Influence of Nitrogen Concentration on Grain Growth, Structural and Electrical Properties of Sputtered Aluminum Nitride Films, *Scr. Mater.*, 2006, **54**, p 1755–1759
23. H. Matthews, *Surface Wave Filters*, Wiley Publication, New York, 1977, p 273
24. C. Campbell, *Surface Acoustic Wave Devices and Their Signal Processing Applications*, Academic Press Inc., 1989, p 80
25. H.H. Kim, B.K. Ju, Y.H. Lee, S.H. Lee, J.K. Lee, and S.W. Kim, Fabrication of Suspended Thin Film Resonator for Application of RF Bandpass Filter, *Microelectron. Reliab.*, 2004, **44**, p 237–243
26. N. Fujitsuka, K. Hamaguchi, H. Funabashi, E. Kawasaki, and T. Fukada, Silicon Anisotropic Etching without Attacking Aluminum with Si and Oxidizing Agent Dissolved in TMAH Solution, *Sens. Actuators A*, 2004, **114**, p 510–515
27. G. Yan, P.C.H. Chan, I.M. Hsing, R.K. Sharma, J.K.O. Sin, and Y. Wang, An Improved TMAH Si-Etching Solution without Attacking Exposed Aluminum, *Sens. Actuators A*, 2001, **89**, p 135–141
28. U. Schnakenberg, W. Benecke, and P. Lange, *IEEE International Conference on Solid-State Sensors and Actuators*, June 24–27, 1991, p 815–818